C. T.-C. Nguyen and R. T. Howe, "CMOS micromechanical resonator oscillator," *Technical Digest*, IEEE International Electron Devices Meeting, Washington, D. C., December 5-8, 1993, pp. 199-202.

CMOS Micromechanical Resonator Oscillator

Clark T.-C. Nguyen and Roger T. Howe

Berkeley Sensor & Actuator Center
Department of Electrical Engineering and Computer Sciences
and the Electronics Research Laboratory
University of California at Berkeley
Berkeley, California 94720

ABSTRACT

A completely monolithic high-Q oscillator, fabricated via a combined CMOS plus surface micromachining technology, is described, for which the oscillation frequency is controlled by a polysilicon micromechanical resonator to achieve stability and phase noise performance comparable to those of quartz crystal oscillators. It is shown that the closed-loop, steady-state oscillation amplitude of this oscillator can be controlled through the dc-bias voltage applied to the capacitively driven and sensed μresonator. Measurements indicate a phase noise density level of -168 dBm/Hz at 5 kHz offset frequency for an oscillator carrier power of -14.5 dBm.

I. INTRODUCTION

Crystal oscillators are widely used to generate precision frequency standards for complex integrated circuits. With the current trend to include increasing amounts of a total system on a single silicon chip, designers have begun to include the oscillator function, sans the crystal, on the silicon die. A completely monolithic high-Q oscillator, however, which includes the "crystal" as well as sustaining CMOS electronics on-chip, is so far unavailable.

The advent of surface micromachining, however, makes possible the implementation of high-Q mechanical resonance on-chip with frequency selectivity comparable to quartz. Polysilicon micromechanical resonators [1], such as shown in Fig. 1, can have Q's over 80,000 [2] and temperature coefficients in the range of -10 ppm/^{o}C (several times less with nulling techniques) [3]. Flexibility in geometry allows for multiple ports and a variety of drive and sense topologies.

A technology which combines planar CMOS processing and surface micromachining can then be used to fabricate a high-Q, mechanically-referenced oscillator completely monolithically.This paper details the design, fabrication, and performance of such an oscillator, integrated with and referenced to a capacitively driven and sensed, folded-beam μmechanical resonator (Fig. 2).

II. OSCILLATOR DESIGN

The equivalent circuit for a two-port μmechanical resonator, shown transformed to an equivalent LCR representation, is presented in Fig. 3 [4]. Comparison of the given element values with those of quartz crystal units (R_x=50Ω, C_x=0.04 pF, L_x=0.25 H) reveals orders of magnitude differences, which dictate differing strategies in the design of μresonator oscillators versus macroscopic crystal oscillators.

The large μresonator series resistance is to some degree a welcome advantage for μresonator-controlled oscillators, since it serves to increase their frequency and phase stabilities by minimizing Q-loading. For example, in a series resonant oscillator, Q-reduction is determined by the size of the resistance in series with the μresonator, which should be small compared with the μresonator for minimal Q-loading. The large R_x of a capacitively driven and sensed μresonator, thus, greatly minimizes Q-reduction in series resonant oscillators. The same applies for parallel resonant oscillators, such as the popular Pierce architecture.

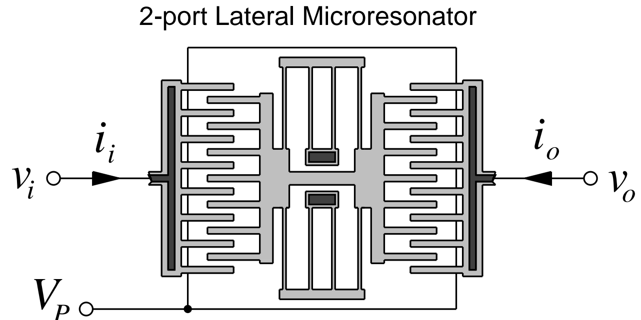

Fig. 1: Overhead view of a two-port, folded-beam, electrostatic-comb driven micromechanical resonator with typical applied bias and excitation voltages.

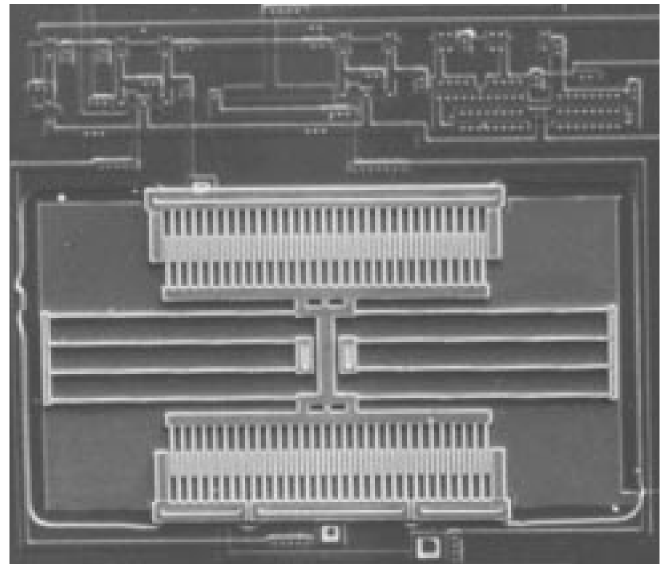

Fig. 2: SEM of the integrated CMOS μresonator oscillator.

One drawback of the larger R_x is the requirement for more gain, and thus more power dissipation, from the amplifier sustaining oscillation. This becomes especially costly for Pierce designs, which are somewhat power inefficient to begin with [5].

In this work, we investigate series resonant designs. Figure 4 shows the circuit schematic for the oscillator of Fig. 2. The sustaining amplifier design is transresistance, using shunt-shunt feedback to achieve a low input resistance, and

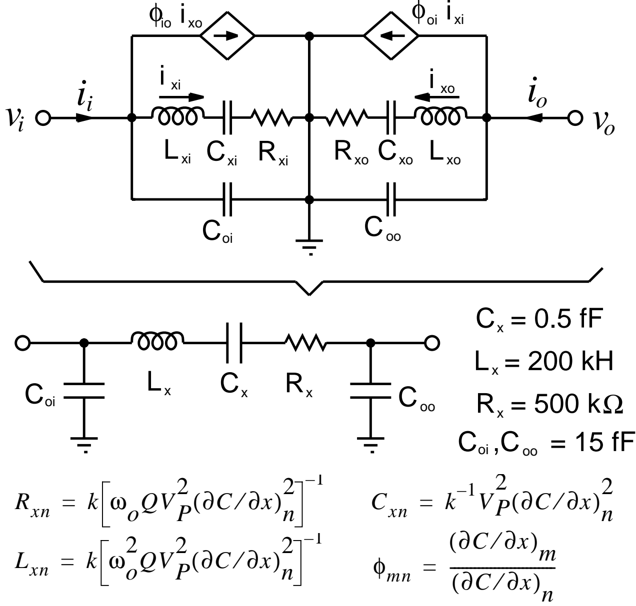

Fig. 3: Equivalent circuit for a two-port μresonator showing the transformation to the more convenient LCR form. In the equations, k is the system spring constant and $(\partial C/\partial x)_n$ is the change in capacitance per displacement at port n of the μresonator.

therefore, minimal Q-loading. M_4 and M_5 serve as replica biasing for gain stages M_1-M_2 and M_6-M_7. M_3 is biased in the linear region by control voltage V_{GC} and serves as an MOS resistor with resistance given by

$$R_3 = \left[\mu_n C_{ox} \frac{W}{L}(V_{GS} - V_t - V_{DS})\right]^{-1}, \quad (1)$$

where μ_n is the electron mobility in silicon, C_{ox} is the gate oxide capacitance per unit area, W and L are the MOS channel width and length, respectively, and V_t is the transistor threshold voltage. The transresistance gain R_{amp} of the amplifier is given by

$$R_{amp} = g_{m7}(r_{o7} \parallel r_{o6})R_3, \quad (2)$$

where g_{m7} is the transconductance of M_7, and r_{o6} and r_{o7} are the output resistances of M_6 and M_7, respectively. To insure start-up of oscillation, the gain R_{amp} should be chosen three

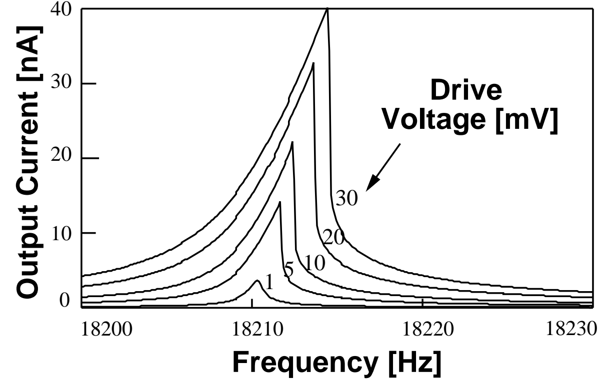

Fig. 5: Measured transconductance spectra for a μresonator under increasing values of applied excitation voltage. The frequency was swept downwards during measurement.

or more times larger than the effective series resistance of the microresonator.

III. AMPLITUDE LIMITING

Oscillation builds up until either some form of nonlinearity or a designed automatic-level control circuit limits the amplitude. For oscillators controlled by quartz crystals, the nonlinearity usually appears in the sustaining circuit, where transistors enter the triode region at large voltage amplitudes, reducing effective device transconductances until the loop gain drops to unity. Limiting due to crystal nonlinearity is rare, since quartz crystal units display very little nonlinearity over normal oscillator operating voltage ranges [6].

On the other hand, limiting due to nonlinearity in flexural-mode μresonators is quite practical through adjustment of the dc-bias voltage V_P (Fig. 1). This can be shown by studying the influences of V_P and resonator nonlinearity on the equivalent series resistance of the μresonator.

Although the use of electrostatic-comb drive and folded beams greatly linearizes the resonator transconductance function over comparable clamped-clamped, parallel-plate driven resonators, the nonlinearity is still several times greater than in high-Q quartz crystals. This nonlinearity is caused by a combination of mechanical spring stiffening and effective electrical spring softening due to comb-drive nonidealities [7]. The degree of nonlinearity can be extracted

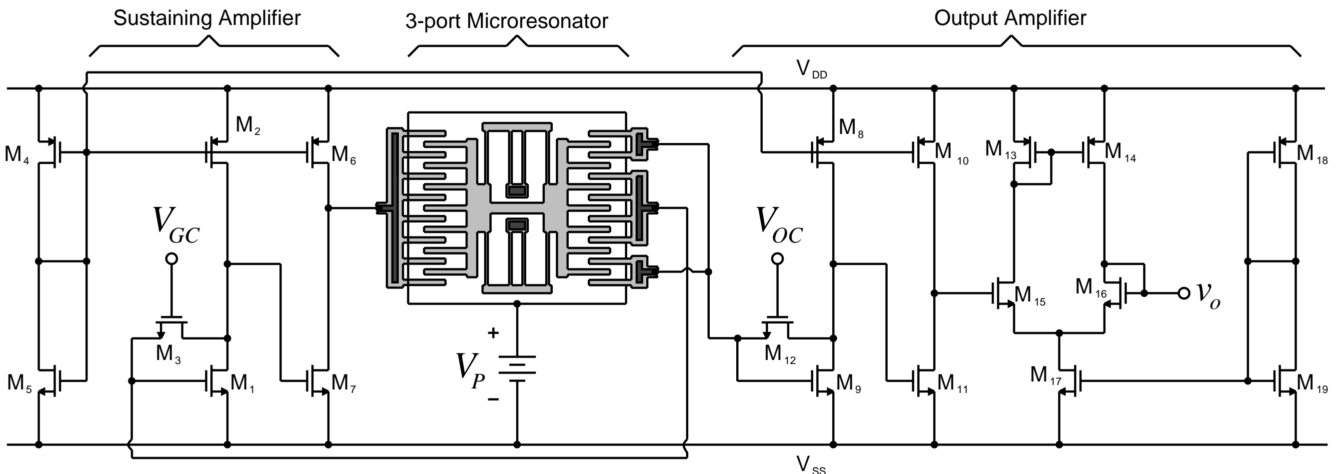

Fig. 4: Circuit schematic for the μresonator oscillator.

from measured Duffing curves, such as those shown in Fig. 5 for a typical comb-driven, folded-beam μresonator. The extraction is based upon the Duffing equation, which models the nonlinear spring as $f_{spring}=k_1x+k_3x^3$, where x is the resonator shuttle displacement and k_1 is the small displacement spring constant. Using Fig. 5, the extracted spring force coefficients for this particular resonator are k_1=0.6 Nm^{-1} and k_3=1.3 × 10^7 Nm^{-3}. The above spring force information may now be used to calculate the voltage amplitude during steady-state oscillator operation, by determining the equivalent series resistance of the microresonator as a function of voltage amplitude. This may be achieved by first performing a series reversion on f_{spring}, transforming amplitude variables from drive force $|f_d|$ to voltage $|v_i|$ and from displacement $|x|$ to current $|i_x|$, and differentiating, yielding a small-signal resistance, R_{ss}, given by

$$\frac{\partial|i_x|}{\partial|v_i|} = \frac{Q}{k_1}\omega_o V_P^2\left(\frac{\partial C}{\partial x}\right)^2 - \frac{81}{64}\frac{k_3 Q}{k_1^4}\omega_o V_P^4\left(\frac{\partial C}{\partial x}\right)^4|v_i|^2 = \frac{1}{R_{ss}} \qquad (3)$$

Equation (3) shows that as the amplitude of oscillation $|v_i|$ grows, the small-signal series resistance R_{ss} increases until it equals the transresistance of the sustaining amplifier, R_{amp}, at which point the loop gain is unity, and $|v_i|$ settles at a steady-state value. From (3), the steady-state $|v_i|$ is clearly controllable through the resonator dc-bias voltage V_P.

IV. PHASE NOISE PERFORMANCE

One important figure of merit for oscillators, particularly those used in communications applications, is the phase noise power present at frequencies close to the carrier frequency. This noise power may be predicted theoretically using the circuit diagram of Fig. 4, and by accounting for the increase in Q (and decrease in bandwidth) for the circuit under positive feedback.

For the case of micro-scale resonator oscillators, however, we need account for not only noise contributions from the sustaining amplifier, but also, from Brownian motion of the micromechanical resonator, which becomes significant at this scale. Using the thermal equilibrium arguments of [8], the noise force power acting on the resonator can be expressed as

$$\frac{\overline{f_n^2}}{\Delta f} = \frac{4kk_BT}{\omega_o Q} \qquad (4)$$

where k is the (small displacement) system spring constant and k_B is Boltzmann's constant. The corresponding displacement noise power will have a biquadratic bandpass dependence upon frequency, consistent with the response of the resonator. However, since the Q of the positive feedback system is much higher than that of the resonator, only the displacement noise power amplitude at resonance is required for the present analysis. Thus, given that $x=Qf_n/k$ at resonance, and $i_x=\omega_o V_P(\partial C/\partial x)x$, the equivalent current noise generator at the output of the microresonator is

$$\frac{\overline{i_x^2}}{\Delta f} = \left[\frac{1}{k}\omega_o V_P^2\left(\frac{\partial C}{\partial x}\right)^2 Q\right](4k_BT) = \frac{4k_BT}{R_x} \qquad (5)$$

where R_x is the series resistance of the micromechanical resonator, as given in Fig. 3. This adds to the equivalent input current noise generator of the transresistance amplifier, given by $\overline{i_r^2}/\Delta f = 4k_BT/R_3$, giving a total equivalent input noise current $i_a=i_x+i_r$.

Proceeding with the analysis, using the above results and following a procedure similar to that in [9], the equation for the relative oscillator phase noise density N_{op} to carrier C power ratio at a deviation f_m from carrier frequency f_o can be written

$$\left.\frac{N_{op}}{C}\right|_{\delta f = f_m} = \frac{(\overline{i_a^2}/\Delta f)R_{amp}^2}{R_L R_{in} C}\frac{1}{8Q^2}\left(\frac{f_o}{f_m}\right)^2. \qquad (6)$$

where R_{in} and R_L are the input and load resistances, respectively. The above assumes a linear oscillator, so $1/f$ mixed noise has been neglected. Note from (6) that the thermal noise contribution from the resonator may degrade oscillator phase noise performance by as much as 3 dB over the performance achieved if resonator noise was not important.

V. FABRICATION

The oscillators were fabricated using a technology that combines planar CMOS processing with surface micromachining [10]. This process features a modular combination of the two technologies, in which the CMOS processing and surface micromachining are done in separate process modules, with no intermixing of CMOS or micromachining steps. This Modular Integration of CMOS and microStructures (MICS) process has the advantage in that it allows the use of nearly any CMOS process with a variety of surface micromachining processes.

A key feature in this process is the use of tungsten metallization with $TiSi_2$ drain/source contact barriers, rather than aluminum, to allow for post-CMOS micromachining processing with temperatures up to 835°C. Structural polysilicon

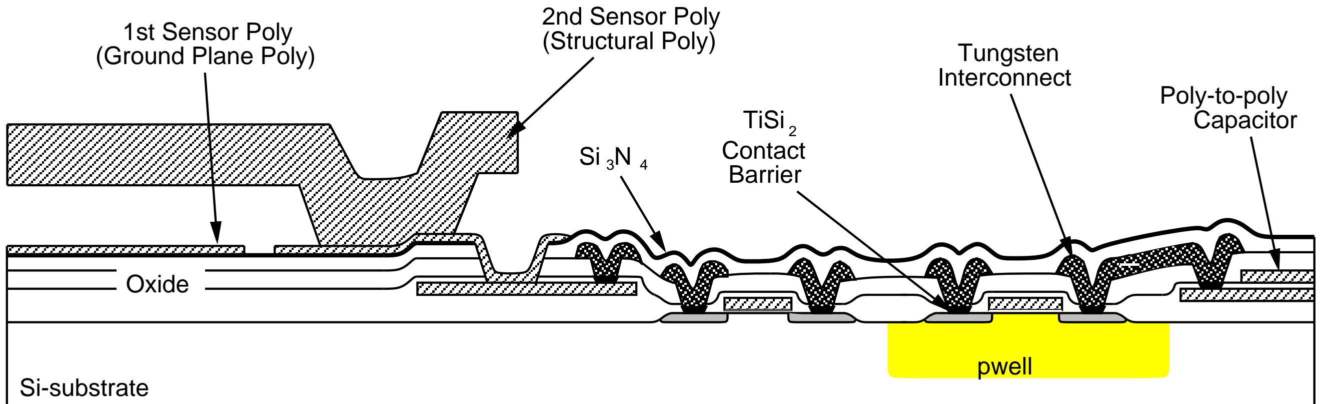

Fig. 6: Cross-section of the MICS technology for integration of CMOS and microstructures.

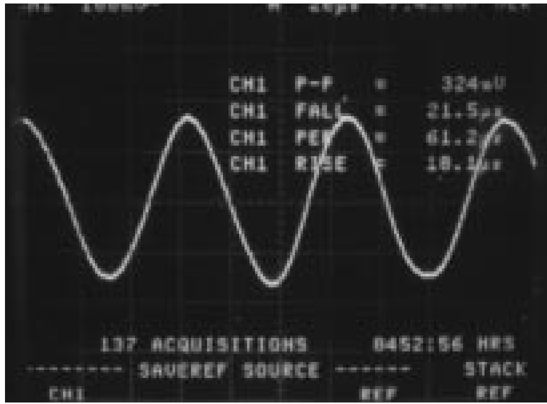

Fig. 7: Oscilloscope waveform for a µresonator oscillator.

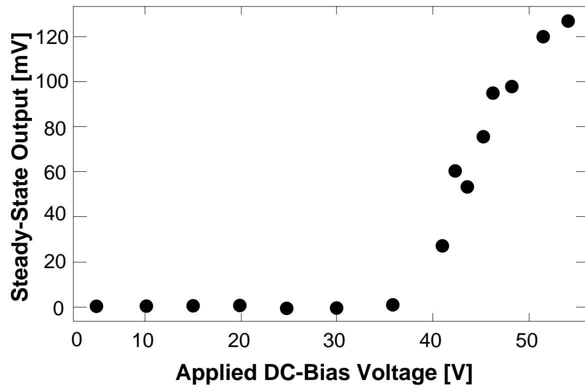

Fig. 8: Measured dependence of oscillator steady-state voltage output amplitude as a function of µresonator dc-bias.

is deposited via *in situ* phosphorous-doped LPCVD and stress annealed via a 30 second rapid thermal anneal (RTA) at 950°C. A cross-section of the MICS technology is presented in Fig. 6.

VI. EXPERIMENTAL RESULTS

Figure 7 shows a typical oscilloscope plot for a 16.5 kHz version of this oscillator. The amplitude of oscillation was visibly controllable through adjustment of V_P, consistent with the discussion of Section III. A measured plot of steady-state oscillator output voltage versus µresonator dc-bias is presented in Fig. 8.

Due to the low frequency of operation for this oscillator, the phase noise density as predicted by (6) is quite small, and is not measurable using available equipment. Thus, rather than measure the phase noise of the oscillator itself, we measure the phase noise of the frequency-multiplied oscillator output signal. Frequency multiplication degrades the oscillator phase noise performance according to the following equation [9]:

$$\left(\frac{N_{op}}{C}\right)_{mult} = n^2\left(\frac{N_{op}}{C}\right)_{osc}, \qquad (7)$$

where $(N_{op}/C)_{mult}$ is the phase noise density to carrier ratio after frequency multiplication by a factor n, and $(N_{op}/C)_{osc}$ is the ratio before multiplication.

The phase noise power density was measured using the set-up shown in Fig. 9. Here, the oscillator frequency was multiplied by 652 to lock to a 10 MHz voltage-controlled crystal oscillator reference, which when subsequently mixed with the µresonator oscillator carrier of power -14.5 dBm,

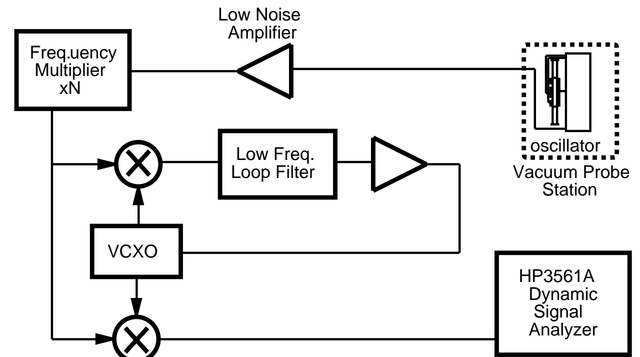

Fig. 9: Schematic diagram of the system used to measure phase noise in the µresonator oscillator.

yields a phase noise power density of -111.8 dBm/Hz at a 5 kHz offset from the carrier. This multiplied noise power density corresponds to a source noise power density (using (7)) of -168 dBm/Hz, which is comparable to that achievable by quartz crystal oscillators.

VII. CONCLUSIONS

Completely monolithic, highly stable, high-*Q* oscillators utilizing surface-micromachined polysilicon mechanical resonators have been designed, fabricated, and tested with particular attention to amplitude control and phase noise performance. Due to the novelty of the process and the devices, conservative measures were taken for the designs, and oscillators up to only 100 kHz were fabricated. Designs up to a few megaHertz are feasible using folded-beam resonator designs, and higher frequencies (tens of MHz) should be feasible using more advanced designs aimed at maximizing resonator quality factor, which would otherwise degrade with increasing frequency. Even higher frequencies may still be generated through frequency multiplication. With phase noise and stability performance comparable to crystal oscillators, microresonator oscillators make the possibility of single-chip communications equipment much more feasible.

Acknowledgments. The authors would like to thank Shenqing Fang for assistance in CMOS fabrication, as well as Katalin Voros and the staff of the Berkeley Microfabrication Laboratory for process support. This research was supported by the Berkeley Sensor & Actuator Center (BSAC).

References:

[1] W. C. Tang et al., *Sensors and Actuators,* **BA21-A23**, pp. 328-331, 1990.

[2] C. T.-C. Nguyen et al., *IEDM Tech. Digest*, pp. 505-508, 1992.

[3] C. T.-C. Nguyen et al., *Transducers'93 Tech. Digest*, pp. 1040-1043, 1993.

[4] C. T.-C. Nguyen, M.S. Report, Univ. Calif. Berkeley, 199l.

[5] E. A. Gerber et al., *Precision Frequency Control*, vol. 2, 1985.

[6] F. L. Walls et al., *IEEE Trans. Ultrason. Ferroelec. Freq. Contr.*, vol. 39, no. 2, pp. 241-249, March 1992.

[7] L.-S. Fan et al., *Transducers'93 Tech. Digest*, pp. 767-770, 1993.

[8] T. B. Gabrielson, *IEEE Trans. Electron Devices*, vol. 4, no. 5, pp. 903-909, May 1993.

[9] W. P. Robins, *Phase Noise in Signal Sources*, 1982.

[10] W. Yun, *IEEE Solid-State Sensor & Actuator Workshop Tech. Digest*, pp. 126-131, 1992.